Cross-sectional and Confining System Unification on Peak compressive strength of FRP confined Concrete

Javad Shayanfar [1], Joaquim A. O. Barros [2] and Mohammadali Rezazadeh [3]

[1] PhD Candidate, ISISE, Department of Civil Engineering, University of Minho, Azurém 4800-058 Guimarães, Portugal, id8287@alunos.uminho.pt (corresponding author)

[2] Full Prof., ISISE, IBS, Department of Civil Engineering, University of Minho, Azurém 4800-058 Guimarães, Portugal, barros@civil.uminho.pt

[3] Lecturer, Civil Eng., Department of Mechanical and Construction Engineering, Northumbria University, Newcastle upon Tyne, NE1 8ST, United Kingdom, mohammadali.rezazadeh@northumbria.ac.uk

Abstract

Despite the many axial confinement models already proposed for the determination of the peak compressive strength of Fiber-Reinforced Polymer (FRP) confined concrete columns, they are, in general, applicable only to concrete columns of circular or square cross-section, with full or partial confinement arrangements. In this study, by proposing a cross-sectional and confining system unification approach, a new model is developed and calibrated based on a large test database. For the generalization of the cross-section and FRP-based confinement arrangement, the concept of confinement efficiency factor with a unified mathematical framework is adopted. By simulating experimental tests and comparing to the predictions of existing confinement models, the developed one demonstrates a very high reliability and suitable for design purposes by balancing the simplicity of the usage and accuracy.

Keywords: FRP-confined concrete; Peak compressive strength; Partial confinement; Square cross-section; Unified model;

1- Introduction

In the past two decades, many studies have been conducted on the behavior of Fiber-Reinforced-Polymer (FRP) confined concrete column under uniaxial compression loadings, where the column response in terms of load-carrying and deformation capacities and energy dissipation can be upgraded proficiently, dependent on an adequate design circumstances [1-9].

For the case of FRP fully confined concrete columns (FFCC as illustrated in Fig. 1), Valdmanis *et al.* [1] experimentally evidenced the reliability of full confinement arrangement in the enhancement of axial and dilation behavior, depending upon FRP volumetric ratio, where improvements were more pronounced for normal-strength concrete columns than high-strength concrete ones. It is well-documented from experimental evidence that the application of FRP wrapping solution for circular cross-section concrete columns (FFCC) is more effective than its application for the case of square cross-section ones (FFSC in Fig. 1a) due to the detrimental effect of the corner radius (r), which is generally known as shape effect induced by horizontal arching action phenomenon. Experimental studies (Shan *et al.* [2]) evidenced that by decreasing the corner radius ratio ($R_b = 2r/b$ where b is the length of section side) from one (representing a circular cross-section) to zero (representing a square cross-section with sharp edge), the efficiency of confinement strategy decreases significantly. On the other hand, since the usage of fully FRP confining configuration in real cases of strengthening might not be cost competitive, the application of a partially confining strategy can be regarded as a reliable alternative under adequate design circumstances. Barros and Ferreira [3] evidenced experimentally that, although the effectiveness of FRP partial confinement system applied to circular column (FPCC in Fig. 1b) is smaller than of a full confining system (FFCC) due to vertical arching action effect, a still significant level of load carrying capacity can be obtained, depending on the distance between FRP strips (s_f) and existing steel hoops. For the case of

FRP partially confined square concrete elements (FPSC in Fig. 1b), Guo *et al.* [4,5] experimentally demonstrated that FRP thickness-induced enhancements in terms of peak axial compressive strength are quite marginal for the cases with largely-spaced FRP strips.

In order to predict peak axial compressive strength (f_{cc}), a variety of confinement models has been proposed (i.e. [10-20]). Nonetheless, most of the models are only reliable and applicable to concrete columns of circular or square cross-section with full or partial confinement arrangements. Considering circular cross-section as a special case for square column where $R_b = 1$, and full confinement arrangement as a special case of partially confining configuration where $s_f = 0$, the reliability of these models for various confinement scenarios is, at least, arguable. Accordingly, a more-reliable model, which is inevitably established by regression analysis technique, can be calibrated/developed through cross-sectional and confining system unification. Few models generalized for FFCC, FFSC, FPCC and FPSC have been proposed in the literature for the calculation of peak axial compressive strength (i.e. CNR DT 200/2004 [12] and *fib* [13]). In these models, for the purpose of unification, the concept of confinement efficiency factor is adopted to take into account the effect of vertical and horizontal arching action. Furthermore, in general, most of the existing models was calibrated by using test database with limited variables i.e. concrete properties, specimen size, corner radius ratio, FRP confinement configuration. Consequently, statistical assessment and subsequently recalibration of these models based on a more comprehensive and larger database would be necessary for enhancing their predictive performance.

In this study, a new model is developed to predict the peak compressive strength (f_{cc}) with a unified character for FFCC, FFSC, FPCC and FPSC under axial loading. For this purpose, a comprehensive database was compiled comprising 1528 FFCC, 308 FFSC, 171 FPCC, and 23 FPSC registered experimentally in the literature. This model adopts the concept of confinement efficiency factor for the generalization of the cross-section and confining system, which is

calibrated based on the collected database. The model validation is demonstrated, and its predictive performance is compared to the one of other existing models.

2- Test Database

To evaluate the reliability of existing models using statistical analysis, a large test database was built, including 2031 FRP confined concrete column specimens tested under axial compressive loading. This database includes 1528 fully confined specimens of circular cross-section (FFCC), 308 fully confined specimens of square cross-section (FFSC), 171 partially confined specimens of circular cross-section (FPCC), and 23 partially confined specimens of square cross-section (FPSC). Specimens in the following conditions were not included in the database: i) having internal transverse and longitudinal steel reinforcements; ii) having helicoidal FRP wrapping confinement configurations; iii) with incomplete information, such as mechanical properties of the intervenient materials; iv) with premature FRP debonding; v) with hybrid confining systems (application of different FRP sheets) for the confinement; vi) under eccentric axial loading; vii) with a peak strength less than the one of its unconfined counterpart.

Table 1 presents the details of the assembled database of FFCC, FPCC, FFSC and FPSC with a wide range of key parameters. As shown, the axial compressive strength of unconfined concrete (f_{c0}) varies from 6.6 to 240 MPa with the mean and CoV values of 44.1 MPa and 0.69, respectively. The confinement-induced improvement (f_{cc}/f_{c0}) is in the range of 1.0 to 6.9 with mean and CoV of 1.9 and 0.424, respectively. The diameter of the circular columns or cross-section edge width (*b*) varies from 50 to 400 mm with the mean and CoV values of 149 mm and 0.296, respectively. The height of the column specimens (*L*) varies from 100 to 1200 mm with the mean and CoV values of 322 mm and 0.383, respectively. The database comprises specimens wrapped with carbon (CFRP), basalt (BFRP), aramid (AFRP), glass (GFRP), polyethylene naphthalate (PEN) and polyethylene terephthalate (PET) fibers. The

elastic modulus of the confining FRP (E_f) is in the range of 9.5 to 657 GPa with the mean and CoV values of 177.7 MPa and 0.572, respectively. The ultimate tensile strain (ε_{fu}) varies between 0.004 to 0.10 with mean and CoV of 0.024 and 0.791, respectively. For the case of partial confinement configuration, the database covers test specimens with various R_f and s_f/b ranging from 0.05 to 0.75. For the case of square cross-section column specimens, the corner radius ratio varies from 0.0 to 0.8.

3- Existing Models

Table 2 represents the existing models developed for the prediction of peak axial strength of FRP confined concrete. These models adopted different methodologies for developing/calibrating their performance in terms of the normalized peak axial strength (f_{cc}/f_{c0}). The formulations of these models can be generally classified into four categories based on: i) the relation of f_{cc}/f_{c0} and the normalized confinement pressure corresponding to FRP rupture ($f_{l,rup}/f_{c0}$) [13,14]; ii) the relation of f_{cc}/f_{c0} and the normalized confinement pressure corresponding to the FRP ultimate tensile strain ($f_{l,u}/f_{c0}$) [15-17]; iii) the development of a relation in which f_{cc}/f_{c0} is as a function of the normalized confinement stiffness ($\rho_K = f_{l,rup}\varepsilon_{c0}/f_{c0}\varepsilon_{h,rup}$ where ε_{c0} is the axial strain corresponding to f_{c0}; $\varepsilon_{h,rup}$ is the FRP hoop strain corresponding to rupture) and FRP strain ratio ($\rho_\varepsilon = \varepsilon_{h,rup}/\varepsilon_{c0}$) [4,5]; iv) the development of a regression-based relation in which f_{cc}/f_{c0} is determined based on the best-fit with respect to key parameters [18]. Among these models, few ones [4,5,12-14] were developed with a unified character for all FFCC, FFSC, FPCC and FPSC cases based on the confinement efficiency factor (k_h and k_v) reflecting the effect of horizontal and vertical arching actions. The models developed by [14, 16-18] are applicable to FFCC and FFSC

through cross-section unification i) by using k_h [14] or ii) by empirically modelling the shape effect according to corner radius ratio (R_b) [16-18].

4- Proposed Model

In this section, a new model is proposed for the determination of f_{cc} based on cross-sectional and confining system unification approach. The procedure to establish the unified model is briefly presented as follows:

i) Adopting the concept of equivalent circular cross-section to convert a square into a circular column's cross section;

ii) Adopting the concept of confinement efficiency factor to reflect the effect of arching action phenomenon in both transversal and longitudinal directions of the column;

iii) Establishment of the relation between normalized peak axial strength (f_{cc}/f_{c0}) with respect to normalized equivalent confinement pressure corresponding to FRP rupture stage ($f_{l,rup}/f_{c0}$).

In the present study, the diameter of the equivalent circular column (D_{eq}) is determined based on the *fib* [13]'s recommendation where D_{eq} is assumed equal to the section dimension b (Fig. 1) for the case of square cross-section ($D_{eq} = b$).

4.1- Concept of Confinement Efficiency Factor

For the simulation of the effect of vertical and horizontal arching actions, due to the presence of ineffective confinement regions, the concept of confinement efficiency factor is followed. By using this concept, the entire cross-section can be considered as effectively and uniformly confined at longitudinal and transversal directions. Based on experimental observations and

finite element simulations, Shayanfar *et al.* [21] proposed a new model to formulate the effect of horizontal arching action on the determination of the equivalent confinement pressure. As shown in Fig. 2a, the original square cross-section was assumed to be subjected to three distinct levels of the confinement pressure:

i) Area III under the lowest confinement level, which was assumed to be marginal ($f_l^{III} = 0$);

ii) Area II under a moderate level of confinement pressure (f_l^{II}), which was assumed equal to $f_l^{II} = 0.5\left(f_l^{I} + f_l^{III} \right) = 0.5 f_l^{I}$;

iii) Area I under the highest level of confinement pressure (f_l^{I}).

Based on equilibrium of lateral forces in the equivalent circular cross-section, Shayanfar *et al.* [21] recommended the highest level of confinement pressure (f_l^{I}) as follows:

$$f_l^{I} = 2\frac{w_f n_f t_f}{\left(w_f + s_f\right) D_{eq}} E_f \varepsilon_h \tag{1}$$

where n_f is the number of FRP layers per strip; t_f is the nominal thickness of a FRP layer; E_f is the FRP modulus of elasticity. In Fig. 2b, $f_{l,eff}$ defines the effective confinement pressure uniformly acting on the region out of the parabolas (Area I and Area II), which was considered proportional to f_l^{I}, dependent on the reduction factor $k_{h,eff}$. Consequently, by using $k_{h,eff}$, the stress field within the confined Areas I and II is converted to an effective confinement pressure ($f_{l,eff}$) uniformly distributed in these areas. Assuming $k_{h,eff}$ on the interval 0.5 and 1 corresponding to the cases of $R_b = 0$ and $R_b = 1$, respectively, Shayanfar *et al.* [21] suggested this reduction factor as:

$$k_{h,eff} = 0.5\left(1 + 2R_b - R_b^{\,2}\right) \tag{2}$$

Fig. 2c shows that using another reduction factor $k_{h,f}$, the effective confinement pressure ($f_{l,eff}$) can be distributed on the entire equivalent circular cross-section, leading to the uniform confinement pressure ($f_{l,i} = k_{h,f}\, f_{l,eff} = k_{h,f} k_{h,eff}\, f_l^{\,I}$). Adopting the concept of the equivalent circular section to convert Area I and Area II into an equivalent circular core with a diameter $D_{eq,c}$, Shayanfar *et al.* [21] suggested this reduction factor to be dependent on R_b as:

$$k_{h,f} = \frac{D_{eq,c}}{D_{eq}} \simeq 1.17R_b - 0.46R_b^{\,2} + 0.29 \tag{3}$$

Accordingly, by defining the confinement efficiency factor (k_h) due to horizontal arching action as $k_{h,f} k_{h,eff}$, it can be determined as:

$$k_h = k_{h,f} k_{h,eff} = 0.5\left(1 + 2R_b - R_b^{\,2}\right)\left(1.17R_b - 0.46R_b^{\,2} + 0.29\right) \tag{4}$$

which can be simplified to:

$$k_h \simeq 0.15 + 0.93R_b \le 1 \tag{5}$$

without significant loss of accuracy. Accordingly, by using k_h, the equivalent uniform confinement pressure acting on the entire section can be expressed as:

$$f_{l,i} = k_h f_l^{\,I} = 2k_h \frac{w_f n_f t_f}{\left(w_f + s_f\right) D_{eq}} E_f \varepsilon_h \tag{6}$$

On the other hand, for the case of partial confinement, Shayanfar *et al.* [22] proposed a new reduction factor, k_v, for simulating the effect of vertical arching action due to the non-uniform distribution of actual confinement pressure imposed to the concrete along the column height as

illustrated in Fig. 3. In this figure, f_z and d_z are the distribution function of the confinement pressure and the diameter of the effective confinement region at the clear distance of *x* from the strip, induced by vertical arching action phenomenon. As shown, owing to vertical arching action, the strip region was assumed to be subjected to the highest confinement pressure ($f_{l,i}$), whereas the concrete at the mid-height of two consecutive strips is subjected to lowest confinement pressure ($f_{l,j}$). The average level of confinement pressure uniformly acting along the column height (f_l) can be defined as $f_l = k_v f_{l,i}$, in the compliance with the concept of confinement efficiency factor [23,24].

Accordingly, based on the equilibrium of confinement forces, Shayanfar *et al.* [22] determined k_v as:

$$k_v = \frac{f_{l,i} w_f D_{eq} + 2\int_0^{s_f/2} f_z d_z dx}{f_{l,i}\left(s_f + w_f\right) D_{eq}} = \frac{w_f + s_f\left(1 - \frac{s_f}{D} + 0.43\left(\frac{s_f}{D}\right)^2 - 0.07\left(\frac{s_f}{D}\right)^3\right)}{w_f + s_f} \tag{7}$$

which can be simplified without significant loss of accuracy to:

$$k_v = \frac{w_f + s_f \exp\left(-0.973 R_f\right)}{w_f + s_f} \leq 1 \tag{8}$$

where $R_f = s_f / D_{eq}$. As a result, both components of the confinement efficiency factor, k_h and k_v , can be calculated by using Eq. (5) and Eq. (8), with the design framework. Hence, for the case of partially FRP confined square concrete column (FPSC), considering $f_l = k_v f_{l,i}$, the confinement pressure uniformly imposed to the concrete can be determined using Eq. (6) (Fig. 3b):

$$f_l = k_v f_{l,i} = 2k_v k_h \frac{w_f n_f t_f}{\left(w_f + s_f\right) D_{eq}} E_f \varepsilon_h \tag{9}$$

4.2- Establishment of peak axial strength

This section addresses the determination of the f_{cc} corresponding to the equivalent confinement pressure at the FRP rupture ($f_{l,rup}$). By defining $\varepsilon_{h,rup}$ as FRP rupture strain, the $f_{l,rup}$ can be calculated based on Eq. (9) by considering $D_{eq} = b$:

$$f_{l,rup} = 2k_v k_h \frac{w_f n_f t_f}{\left(w_f + s_f\right) b} E_f \varepsilon_{h,rup} \qquad \text{for } n_f \le 3 \tag{10a}$$

$$f_{l,rup} = 2k_v k_h \frac{w_f n_f^{0.85} t_f}{\left(w_f + s_f\right) b} E_f \varepsilon_{h,rup} \qquad \text{for } n_f \ge 4 \tag{10b}$$

where k_h and k_v can be calculated by Eq. (5) and Eq. (8), respectively. In Eq. (10b), for the case with many FRP layers ($n_f \ge 4$), *fib* [13]'recommendation was followed in order to consider the decrease of FRP jacket confinement effectiveness with the increase of the FRP stiffness above a certain limit. By performing regression analysis on a large test database, Shayanfar *et al.* [25] improved the formulation suggested by Lam and Teng [20], where the effects of f_{c0} and FRP ultimate tensile strain (ε_{fu}) were considered:

$$\varepsilon_{h,rup} = \left(\frac{0.586}{0.82 + 0.23 f_{c0} \varepsilon_{fu}} \right) \varepsilon_{fu} \ge 0.35 \varepsilon_{fu} \tag{11}$$

In the present study, based on the best-fit of the model with the experimental results in the database, as demonstrated in Table 1, a new relation generalized for FFCC, FFSC, FPCC and

FPSC is proposed to calculate f_{cc}, as a function of the normalized confinement pressure ($f_{l,rup}/f_{c0}$):

$$\frac{f_{cc}}{f_{c0}} = 1 + \frac{3.4}{k_r}\left(\frac{f_{l,rup}}{f_{c0}}\right) \qquad \text{for } \frac{f_{l,rup}}{f_{c0}} \geq 0.05 \tag{12a}$$

$$\frac{f_{cc}}{f_{c0}} = 1 \qquad \text{for } \frac{f_{l,rup}}{f_{c0}} < 0.05 \tag{12b}$$

In Eq. (12), when $f_{l,rup}/f_{c0}$ is lower than 0.05, the confinement-induced improvement is neglected. The reduction factor k_r (larger than 1) is proposed to account the stress concentration in square cross section column with almost sharp edge as:

$$k_r = 2.7 - 10R_b \geq 1 \tag{13}$$

As a result, FRP confinement-induced improvement can be calculated through the proposed model with a unified character for different confining arrangements and cross-section columns (FFCC, FFSC, FPCC and FPSC).

It should be noted that in a reinforced concrete (RC) column, a certain level of confinement is provided by steel transverse reinforcements. Accordingly, for the real cases of RC columns wrapped by FRP jacket, the dual internal steel-FRP confinement is imposed to the concrete core. Based on Triantafyllou *et al.* [26] and Lin *et al.* [27], the peak axial strength of FRP confined RC columns (f_{cc}^{Total}) can be assumed as $f_{cc}^{FRP} + \Delta f_{cc}^{Stirrup}$ where $\Delta f_{cc}^{Stirrup}$ is the steel transverse reinforcements' contribution in the combined steel-FRP confinement and f_{cc}^{FRP} can be calculated by the model proposed in the present study. Therefore, by addressing the effect of steel confinement ($\Delta f_{cc}^{Stirrup}$) based on regression analysis performed on an adequate test database, the proposed model can be extended for the case of FRP confined RC columns,

having a unified character with FRP confined concrete (where $\Delta f_{cc}^{Stirrup} = 0$), which will be the focus of a future research study.

5- Statistical assessments

In the present study, to comprehensively evaluate the reliability and predictive performance of existing models (as presented in Table 2), the experimental tests of the assembled database were simulated with these models, and the obtained results were treated by determining the statistical indicators of *Mean Value* (MV in Eq. (14)), *Coefficient of Variation* (CoV in Eq. (15)), *Mean Absolute Percentage Error* (MAPE in Eq. (16)), *Mean Squared Error* (MSE in Eq. (17)), and *R-squared* (R^2 in Eq. (18)):

$$MV = \frac{1}{n}\sum_{1}^{n}\frac{T_i}{E_i} \tag{14}$$

$$CoV = \frac{SD}{MV} \tag{15}$$

$$MAPE = \frac{1}{n}\sum_{1}^{n}\left|1-\frac{T_i}{E_i}\right| \tag{16}$$

$$MSE = \frac{1}{n}\sum_{1}^{n}\left(T_i - E_i\right)^2 \tag{17}$$

$$R^2 = \left(\frac{\sum_{1}^{n}\left[\left(T_i-\bar{T}\right)\left(E_i-\bar{E}\right)\right]}{\sqrt{\sum_{1}^{n}\left[\left(T_i-\bar{T}\right)^2\left(E_i-\bar{E}\right)^2\right]}}\right)^2 \tag{18}$$

where T_i and E_i are f_{cc}/f_{c0} obtained analytically and experimentally, respectively; *SD* is standard deviation; n is the number of data; $\bar{T}$ and $\bar{E}$ represent the mean values of the analytical and experimental predictions, respectively.

Fig. 4 and Table 3 compares the predictive performance of existing and proposed model over 1528 experimental data of FFCC. As evidenced, the proposed model provided close and uniform predictions of experimental counterparts based on the main statistical indicators i.e. CoV = 0.211, MAPE=0.154, MSE = 0.259 and R^2 = 0.864. Even though *fib* [7] (Fig. 4a) and ACI 440.2R-17 [8] (Fig. 4c) provided the best performance among the existing models with slight conservative results, the proposed model has better predictive performance in estimating the experimental f_{cc}/f_{c0}.

For the case of fully FRP confined concrete column of square cross section (FFSC), the predictive performance of proposed and existing models in estimating f_{cc} is compared in Fig. 5 and Table 4. As shown, the proposed and Cao *et al.* [18] models demonstrated the best performance with similar statistical indicator results, and better when compared to the ones of the other models.

For the case of partially FRP confined concrete columns of circular cross section (FPCC), Fig. 6 and Table 5 evidence that the proposed model is able to accurately and uniformly predict the experimental f_{cc}. Even though CNR DT 200/2004 [12] also provided a good estimation of experimental counterparts, the proposed model presented the best predictive performance.

For the case of partially FRP confined concrete columns of square cross section (FPSC), Fig. 7 and Table 6 show that the Guo *et al.* [4,5] and the proposed models have presented the best performance with almost identical results of statistical indicators, and better than those of *fib* [13] and CNR DT 200/2004 [12]. Nonetheless, the predictive performance of the proposed model was better than Guo *et al.* [4,5] in the FFCC, FFSC and FPCC.

The predictive performance of the proposed model is compared in Fig. 8 with the one of the models that have a unified approach for predicting f_{cc} of FFCC, FFSC, FPCC and FPSC,

namely *fib* [13], Guo *et al.* [4,5] and CNR DT 200/2004 [12]. This comparison shows that the proposed model has the best predictive performance in estimating the experimental f_{cc}, confirming its reliability. Among the existing unified models, *fib* [13] prediction also has a good agreement with experimental counterparts.

For further evaluation of the proposed model, its predictive performance was assessed with respect to key parameters, as demonstrated in Fig. 9. As evidenced in Fig. 9a, the model has relatively uniform performance for different level of $f_{l,rup}/f_{c0}$. Fig. 9b shows that, even though the effect of f_{c0} was not considered in the establishment of the relation of f_{cc}/f_{c0} and $f_{l,rup}/f_{c0}$ in Eq. (12), there is not any significant correlation between the error ($f_{cc}^{Ana}/f_{cc}^{Exp}$) with respect to f_{c0}. Fig. 9c also confirms that there is no obvious variation in model prediction with respect to ε_{fu}. In Fig. 9d, the model performance can be also considered uniform for the range of $D_{eq}/150$ of the database. For the case of column of square cross-section (FFSC and FPSC), Fig. 9e shows that the model reveals slight conservative predictions with uniform performance for different level of R_b, where a larger scatter was observed in columns of circular cross section ($R_b = 1$). For the case of partially confined concrete column (FPCC and FPSC), Fig. 9f confirms the uniform error distribution with respect to different ranges of R_f even though there is a larger scatter for full confinement cases with $R_f = 0$. In Figs. 9e and 9f, the reliability of the adopted concept of confinement efficiency factor (k_h and k_v presented in Eq. (5) and Eq. (8), respectively) for the generalization of the cross-section and confining arrangement can also be confirmed.

6- Summary and conclusions

In this study, a new model with a unified approach for being capable of predicting the peak axial compressive strength (f_{cc}) of concrete columns of different confinement arrangements and of circular or square cross sections (FFCR, FPCR, FFCC and FPCC) was developed, and its predictive performance was assessed by using a large database of experimental results, and compared to the one of existing models. For the generalization of the cross-section and confining arrangement, the concept of confinement efficiency factor with a unified mathematical framework was adopted. For statistical assessment and the calibration of the developed model, a comprehensive database comprising 1528 FFCC, 308 FFSC, 171 FPCC, and 23 FPSC experimental results were collected from the literature. The predictive performance was assessed in terms of *Mean Value* (MV), *Coefficient of Variation* (CoV), *Mean Squared Error* (MSE), *Mean Absolute Percentage Error* (MAPE) and *R-squared* (R^2). For the data based composed of 2031 experimental results, the developed model has presented the best statistical predictive indicators amongst the models applicable to FFCR, FPCR, FFCC and FPCC, namely: MV = 0.969, CoV = 0.196, MAPE = 0.143, MSE = 0.214, R^2 = 0.864.

Acknowledgments

This study is a part of the project ‘‘Sticker –Innovative technique for the structural strengthening based on using CFRP laminates with multifunctional attributes and applied with advanced cement adhesives’’, with the reference POCI-01-0247-FEDER-039755’’. The first author also acknowledges the support provided by FCT PhD individual fellowship 2019 with the reference of “SFRH/BD/148002/2019”.

References

1- *Valdmanis, V., De Lorenzis, L., Rousakis, T., Tepfers, R.* Behaviour and capacity of CFRP-confined concrete cylinders subjected to monotonic and cyclic axial compressive load. Structural Concrete, 8(4), 2007, pp. 187-200.

2- *Shan, B., Gui, F. C., Monti, G., Xiao, Y.* Effectiveness of CFRP confinement and compressive strength of square concrete columns. Journal of Composites for Construction, 23(6), 2019, pp. 04019043.

3- *Barros, J. A., Ferreira, D. R.* Assessing the efficiency of CFRP discrete confinement systems for concrete cylinders. Journal of composites for construction, 12(2), 2008, pp. 134-148.

4- *Guo, Y. C., Gao, W. Y., Zeng, J. J., Duan, Z. J., Ni, X. Y., Peng, K. D.* Compressive behavior of FRP ring-confined concrete in circular columns: Effects of specimen size and a new design-oriented stress-strain model. Construction and Building Materials, 201, 2019, pp. 350-368.

5- *Guo, Y. C., Xiao, S. H., Luo, J. W., Ye, Y. Y., Zeng, J. J.*. Confined concrete in fiber-reinforced polymer partially wrapped square columns: axial compressive behavior and strain distributions by a particle image velocimetry sensing technique. Sensors, 18(12), 2018, pp. 4118.

6- *Del Vecchio, C., Di Ludovico, M., Balsamo, A., Prota, A., Cosenza, E.* (2019). Experimental response and fiber-reinforced cement composites strengthening of real reinforced concrete columns with poor-quality concrete. Structural Concrete, 20(3), 1168-1181.

7- *Pantazopoulou, S. J., Tastani, S. P., Thermou, G. E., Triantafillou, T., Monti, G., Bournas, D., Guadagnini, M.* (2016). Background to the European seismic design provisions for retrofitting RC elements using FRP materials. Structural Concrete, 17(2), 194-219.

8- *Nematzadeh, M., Mousavimehr, M., Shayanfar, J., Omidalizadeh, M.* (2021). Eccentric compressive behavior of steel fiber-reinforced RC columns strengthened with CFRP wraps: Experimental investigation and analytical modeling. Engineering Structures, 226, 111389.

9- *Rousakis, T. C., Panagiotakis, G. D., Archontaki, E. E., Kostopoulos, A. K.* (2019). Prismatic RC columns externally confined with FRP sheets and pre-tensioned basalt fiber ropes under cyclic axial load. Composites Part B: Engineering, 163, 96-106.

10- *Ziaadiny, H., Abbasnia, R.* (2016). Unified cyclic stress-strain model for FRP-confined concrete circular, square and rectangular prisms. Structural Concrete, 17(2), 220-234.

11- *Fanaradelli, T., Rousakis, T.* (2021). Assessment of analytical stress and strain at peak and at ultimate conditions for fiber-reinforcement polymer-confined reinforced concrete columns of rectangular sections under axial cyclic loading. Structural Concrete, 22(1), 95-108.

12- CNR-DT 200. Guide for the design and construction of externally bonded FRP systems for strengthening existing structures. Italian National Research Council, 2004.

13- Fib Bulletin 90. Externally applied FRP reinforcement for concrete structures. Task Group 5. 1, International Federation for Structural Concrete, 2019.

14- ACI 440.2R-17. Guide for the design and construction of externally bonded FRP systems for strengthening concrete structures; American Concrete Institute (ACI): Farmington Hills MI USA, 2017.

15- *Fallahpour, A., Ozbakkaloglu, T., Vincent, T.* Simplified design-oriented axial stress-strain model for FRP-confined normal-and high-strength concrete. Engineering Structures, 175, 2018, pp. 501-516.

16- *Wei, Y. Y., Wu, Y. F.* Unified stress–strain model of concrete for FRP-confined columns. Construction and Building Materials, 26(1), 2012, pp. 381-392.

17- *Nisticò, N., Monti, G.* RC square sections confined by FRP: Analytical prediction of peak strength. Composites Part B: Engineering, 45(1), 2013, pp. 127-137.

18- *Cao, Y. G., Jiang, C., Wu, Y. F.* Cross-sectional unification on the stress-strain model of concrete subjected to high passive confinement by fiber-reinforced polymer. Polymers, 8(5), 2016, pp. 186.

19- *Lin, S., Zhao, Y. G., Li, J., Lu, Z. H.* Confining stress path-based compressive strength model of axially loaded FRP-confined columns. Journal of Composites for Construction, 25(1), 2021, pp. 04020077.

20- *Lam, L., Teng, J. G.* Design-oriented stress–strain model for FRP-confined concrete. Construction and building materials, 17(6-7), 2003, pp. 471-489.

21- *Shayanfar, J., Barros, J. A., Rezazadeh, M.* Unified model for fully and partially FRP confined circular and square concrete columns subjected to axial compression. Engineering Structures, 251, 2022, pp. 113355.

22- *Shayanfar, J., Rezazadeh, M., Barros, J. A.* Analytical model to predict dilation behavior of FRP confined circular concrete columns subjected to axial compressive loading. Journal of Composites for Construction, 24(6), 2020, pp. 04020071.

23- *Shayanfar, J., Barros, J. A., Rezazadeh, M.* Generalized Analysis-oriented model of FRP confined concrete circular columns. Composite Structures, 2021, pp. 270, 114026.

24- Shayanfar, J., Rezazadeh, M., Barros, J., & Ramezansefat, H. (2020, March). A new dilation model for FRP fully/partially confined concrete column under axial loading. In RILEM Spring Convention and Conference (pp. 435-446). Springer, Cham.

25- *Shayanfar, J., Rezazadeh, M., Barros, J. A.* Theoretical Prediction of Axial Response of FRP Fully/partially Confined Circular Concrete Under Axial Loading. In International Conference on Fibre-Reinforced Polymer (FRP) Composites in Civil Engineering (pp. 1439-1449). Springer, Cham., 2021.

26- *Lin, G., Yu, T., & Teng, J.* (2016). Design-Oriented Stress-Strain Model for Concrete under Combined FRP-Steel Confinement. Journal of Composites for Construction, 20(4), 4015084.

27- *Triantafillou, G. G., Rousakis, T. C., & Karabinis, A. I.* (2015). Axially loaded reinforced concrete columns with a square section partially confined by light GFRP straps. Journal of Composites for Construction, 19(1), 04014035.

List of Tables

List of Figure

Fig. 2. Distribution of confinement pressure within a square cross-section

Fig. 3. Vertical arching action phenomenon for partially FRP confined concrete

Fig. 4. Axial compressive strength of FFCC: test versus predicted results

Fig. 5. Axial compressive strength of FFSC: test versus predicted results

Fig. 6. Axial compressive strength of FPCC: test versus predicted results

Fig. 7. Axial compressive strength of FPSC: test versus predicted results

Fig. 8. Axial compressive strength of FFCC/FFSC/FPCC/FPSC: test versus predicted results

Fig. 9. Performance of the proposed model with respect to key parameters

Table 1. Summary of the compiled database for FFCC, FPCC, FFSC and FPSC.

Confinement arrangement	Number of datasets		f_{c0} range (MPa)	$\frac{f_{cc}}{f_{c0}}$ range	L range (mm)	b range (mm)	E_f range (GPa)	ε_{fu} range	R_b [a]	R_f [b]
FFCC /FFSC /FPCC /FPSC	**2031**	Min.	6.6	1.0	100	50	9.5	0.004	0.00	0.00
		Max.	204.0	6.9	1200	400	657	0.100	1.00	0.75
		Mean	44.1	1.9	321.8	149.4	177.7	0.024	0.89	0.05
		CoV	0.691	0.424	0.383	0.296	0.572	0.791	0.301	2.663
FFCC	**1529**	Min.	6.6	1.0	100	50	9.5	0.004	1	0
		Max.	204.0	6.9	915	305	657	0.100	1	0
		Mean	47.7	2.1	300.1	144.3	173.4	0.024	1	0
		CoV	0.701	0.417	0.352	0.295	0.614	0.801	0.000	0.000
FFSC	**308**	Min.	8.7	1.0	280	100	9.5	0.009	0.00	0
		Max.	77.2	4.3	1200	400	259.7	0.093	0.80	0
		Mean	33.3	1.6	394.1	168.9	166.8	0.027	0.31	0
		CoV	0.411	0.353	0.402	0.306	0.571	0.799	0.675	0.000
FPCC	**171**	Min.	16.6	1.0	200	100	104.6	0.015	1	0.05
		Max.	101.2	3.1	700	300	259.7	0.019	1	0.75
		Mean	33.5	1.5	353.5	154.9	230.9	0.017	1	0.33
		CoV	0.436	0.284	0.321	0.214	0.153	0.080	0.000	0.542
FPSC	**23**	Min.	12.3	1.0	500	150	73.0	0.015	0.13	0.10
		Max.	34.7	1.4	750	200	259.7	0.028	0.33	0.51
		Mean	28.3	1.22	557.4	183.4	215.7	0.020	0.30	0.24
		CoV	0.287	0.092	0.152	0.107	0.264	0.172	0.129	0.434

a: $R_b = 2r/b$ where *r* is the corner radius of the cross-section; *b* is the cross-section dimension as shown in Fig. 1

b: $R_f = s_f/b$ where s_f is the distance between two adjacent strips as shown in Fig. 1

Table 2. Existing strength models for FRP confined concrete columns

ID	Model expression	Model parameters	Applicability
fib **[13]**	$\frac{f_{cc}}{f_{c0}} = 1 + 3.3\frac{f_{l,rup}}{f_{c0}}$ for $\frac{f_{l,rup}}{f_{c0}} \geq 0.07$ $\frac{f_{cc}}{f_{c0}} = 1$ for $\frac{f_{l,rup}}{f_{c0}} \leq 0.07$	$f_{l,rup} = 2k_h k_v \frac{n_f t_f E_f}{b}\varepsilon_{h,rup}$ for $n_f \leq 3$ $f_{l,rup} = 2k_h k_v \frac{n_f^{0.85} t_f E_f}{b}\varepsilon_{h,rup}$ for $n_f \geq 4$ $k_h = 1 - \frac{2(b-2r)^2}{3b^2}$ $k_v = \left(1 - \frac{s_f}{2b}\right)^2$ $\varepsilon_{h,rup} = \eta_\varepsilon \varepsilon_{fu}$ $\eta_\varepsilon = 0.5\frac{r}{50}\left(2 - \frac{r}{50}\right)$ for $r \leq 60$ mm $\eta_\varepsilon = 0.5$ for $r > 60$ mm	**FFCC** **FFSC** **FPCC** **FPSC**
CNR DT 200/2004 [12]	$\frac{f_{cc}}{f_{c0}} = 1 + 2.6\left(\frac{f_{l,rup}}{f_{c0}}\right)^{\frac{2}{3}}$ for $\frac{f_{l,rup}}{f_{c0}} \geq 0.05$ $\frac{f_{cc}}{f_{c0}} = 1$ for $\frac{f_{l,rup}}{f_{c0}} \leq 0.05$	$f_{l,rup} = \frac{1}{2}k_h k_v \rho_f E_f \varepsilon_{fd.rid}$ $\rho_f = \frac{4n_f t_f}{b}$ for FFCC/FFSC $\rho_f = \frac{4n_f t_f w_f}{s_f b}$ for FPCC/FPSC $k_h = 1 - \frac{2(b-2r)^2}{3b^2}$ $k_v = \left(1 - \frac{s_f}{2b}\right)^2$ $\varepsilon_{fd.rid} = \min\left\{\frac{\eta_a \varepsilon_{fu}}{\lambda_f}, 0.004\right\}$ η_a = 0.65, 0.75 and 0.85 for the fibre/resin type as Glass/Epoxy, Aramid/Epoxy and Carbon/Epoxy, respectively. λ_f = the partial factor recommended as 1.10.	**FFCC** **FFSC** **FPCC** **FPSC**
Guo et al. [4,5]	$\frac{f_{cc}}{f_{c0}} = 1 + 2(\rho_{Ke} - 0.01)\rho_\varepsilon$ for $\rho_{Ke} \geq 0.01$ $\frac{f_{cc}}{f_{c0}} = 1$ for $\rho_{Ke} \leq 0.01$	$\rho_{Ke} = 2k_v \frac{n_f t_f E_f \varepsilon_{c0}}{b f_{c0}}$ for FFCC/FPCC $\rho_{Ke} = 2k_h k_v \frac{n_f t_f E_f \varepsilon_{c0}}{\sqrt{2} b f_{c0}}$ for FFSC/FPSC $\rho_\varepsilon = \frac{\varepsilon_{h,rup}}{\varepsilon_{c0}}$ $\varepsilon_{c0} = 0.000937 f_{c0}^{0.25}$ $k_h = 1 - \frac{2(b-2r)^2}{3b^2}$ $k_v = \left(1 - \frac{s_f}{2b}\right)^2$ $\varepsilon_{h,rup} = 0.568\varepsilon_{fu}$	**FFCC** **FFSC** **FPCC** **FPSC**
ACI 440.2R-17 [14]		$f_{l,rup} = 2\frac{n_f t_f E_f}{b}\varepsilon_{h,rup}$ for FFCC	**FFCC** **FFSC**

	$\frac{f_{cc}}{f_{c0}}=1+3.3\psi_f\frac{f_{l,rup}}{f_{c0}}$ for $\frac{f_{l,rup}}{f_{c0}}\geq 0.08$ $\frac{f_{cc}}{f_{c0}}=1$ for $\frac{f_{l,rup}}{f_{c0}}\leq 0.08$	$f_{l,rup}=2k_h\frac{n_f t_f E_f}{\sqrt{2}b}\varepsilon_{h,rup}$ for FFSC $k_h=1-\frac{2(b-2r)^2}{3b^2}$ $\varepsilon_{h,rup}=0.55\varepsilon_{fu}$	
Fallahpour *et al.* [15]	$\frac{f_{cc}}{f_{c0}}=1+(2.5-0.01f_{c0})\frac{f_{l,u}}{f_{c0}}$	$f_{l,u}=2\frac{n_f t_f E_f}{b}\varepsilon_{fu}$	**FFCC**
Wei and Wu [16]	$\frac{f_{cc}}{f_{c0}}=1+2.2\left(\frac{2r}{b}\right)^{0.72}\left(\frac{f_{l,u}}{f_{c0}}\right)^{0.94}$	$f_{l,u}=2\frac{n_f t_f E_f}{b}\varepsilon_{fu}$	**FFCC** **FFSC**
Nistico and Monti [17]	$\frac{f_{cc}}{f_{c0}}=1+2.2\left(\frac{2r}{b}\right)\frac{f_{l,u}}{f_{c0}}$	$f_{l,u}=2\frac{n_f t_f E_f}{b}\varepsilon_{fu}$	**FFCC** **FFSC**
Cao *et al.* [18]	$\frac{f_{cc}}{f_{c0}}=1+8.34\left(\frac{K_L}{E_c}\right)^{1.03}\left(\frac{2r}{b}\right)^{0.81}\left(\frac{30}{f_{c0}}\right)^{0.54}\left(\frac{\varepsilon_{fu}}{\varepsilon_{c0}}\right)^{0.82}$	$K_L=\frac{2n_f t_f E_f}{b}$ $E_c=4730\sqrt{f_{c0}}$ $\varepsilon_{c0}=0.000937f_{c0}^{0.25}$	**FFCC** **FFSC**
Lin *et al.* [19]	$\frac{f_{cc}}{f_{c0}}=1+2.2\lambda f_{c0}^{0.11}\left(\frac{f_{l,rup}}{f_{c0}}\right)^{0.81}$	$f_{l,rup}=2\frac{n_f t_f E_f}{b}\varepsilon_{h,rup}$ $\lambda=13.2f_{c0}^{-0.95}f_{l,u}^{0.2}\leq 1$ $f_{l,u}=2\frac{n_f t_f E_f}{b}\varepsilon_{fu}$ $\varepsilon_{h,rup}=0.74\varepsilon_{fu}$	**FFCC**

where f_{cc} = peak axial strength of FRP confined concrete; f_{c0} = axial strength of unconfined concrete; $f_{l,rup}$ = confinement pressure corresponding to FRP rupture strain ($\varepsilon_{h,rup}$); $f_{l,u}$ = confinement pressure corresponding to FRP ultimate tensile strain (ε_{fu}); n_f = number of FRP layers; t_f = nominal FRP thickness; k_h = confinement efficiency factor reflecting the effect of horizontal arching action; k_v = confinement efficiency factor reflecting the effect of vertical arching action; ρ_f = FRP reinforcement ratio; ρ_{Ke} = FRP confinement stiffness index; ρ_ε = FRP strain ratio; ε_{c0} = axial strain corresponding to f_{c0}; ψ_f = reduction factor recommended as 0.95; K_L = FRP confinement stiffness per the length of section dimension; E_c = concrete modulus of elasticity;

Table 3. Statistical assessment of existing and proposed models for FFCC

ID	Test data	MV	CoV	MAPE	MSE	R^2
Proposed Model	1529	**0.977**	**0.211**	**0.154**	**0.259**	**0.864**
Lin et al. [19]		1.054	0.285	0.180	0.424	0.713
***fib* [13]**		0.904	0.226	0.182	0.332	0.813
Guo et al. [4,5]		0.771	0.252	0.264	0.634	0.817
Fallahpour et al. [15]		1.039	0.290	0.185	0.472	0.722
ACI 440.2R-17 [14]		0.948	0.273	0.187	0.364	0.807
Cao et al. [18]		1.146	0.298	0.213	0.945	0.757
Nistico and Monti [17]		1.046	0.284	0.188	0.425	0.799
Wei and Wu [16]		1.091	0.275	0.197	0.424	0.808
CNR DT 200/2004 [12]		0.772	0.260	0.261	0.754	0.794

Table 4. Statistical assessment of existing and proposed models for FFSC

ID	Test data	MV	CoV	MAPE	MSE	R^2
Proposed Model	308	**0.934**	**0.153**	**0.126**	**0.102**	**0.816**
***fib* [13]**		0.895	0.172	0.146	0.150	0.795
Guo *et al.* [4,5]		0.867	0.225	0.184	0.240	0.632
ACI 440.2R-17 [14]		0.917	0.212	0.157	0.158	0.670
Cao *et al.* [18]		1.001	0.163	0.125	0.081	0.811
Nistico and Monti [17]		0.893	0.167	0.147	0.158	0.794
Wei and Wu [16]		0.986	0.171	0.128	0.094	0.795
CNR DT 200/2004 [12]		0.872	0.245	0.196	0.297	0.576

Table 5. Statistical assessment of existing and proposed models for FPCC

ID	Test data	MV	CoV	MAPE	MSE	R^2
Proposed Model	171	**0.960**	**0.099**	**0.083**	**0.034**	**0.909**
***fib* [13]**		1.140	0.151	0.169	0.084	0.845
Guo *et al.* [4,5]		0.971	0.156	0.107	0.065	0.850
CNR DT 200/2004 [12]		0.914	0.137	0.127	0.063	0.865

Table 6. Statistical assessment of existing and proposed models for FPSC

ID	Test data	MV	CoV	MAPE	MSE	R^2
Proposed Model	23	**1.013**	**0.067**	**0.053**	**0.010**	**0.971**
***fib* [13]**		1.124	0.085	0.140	0.046	0.950
Guo *et al.* [4,5]		1.029	0.056	0.048	0.009	0.981
CNR DT 200/2004 [12]		1.314	0.172	0.359	0.222	0.929

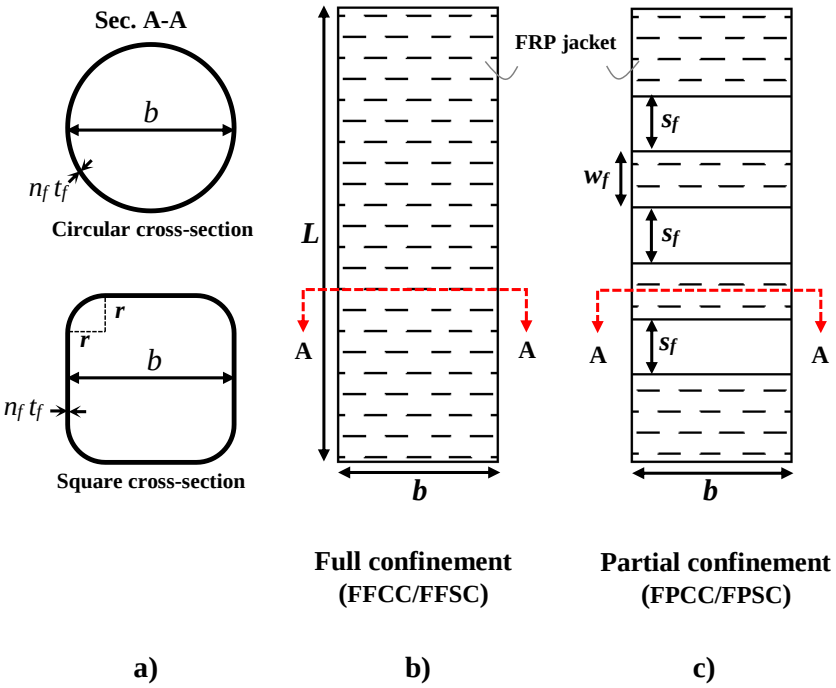

Fig. 1. Concrete columns of a) circular and square cross section (CC, SC) with b) Full confinement arrangements (FFCC/FFSC), and c) partial confinement arrangements (FPCC/FPSC)

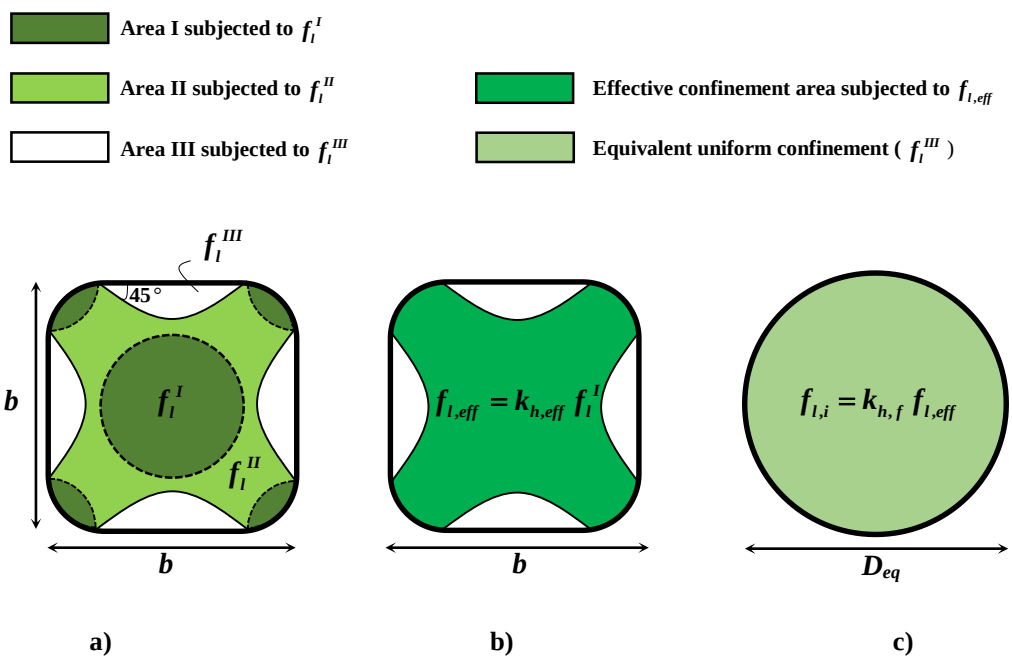

Fig. 2. Distribution of confinement pressure within a square cross-section

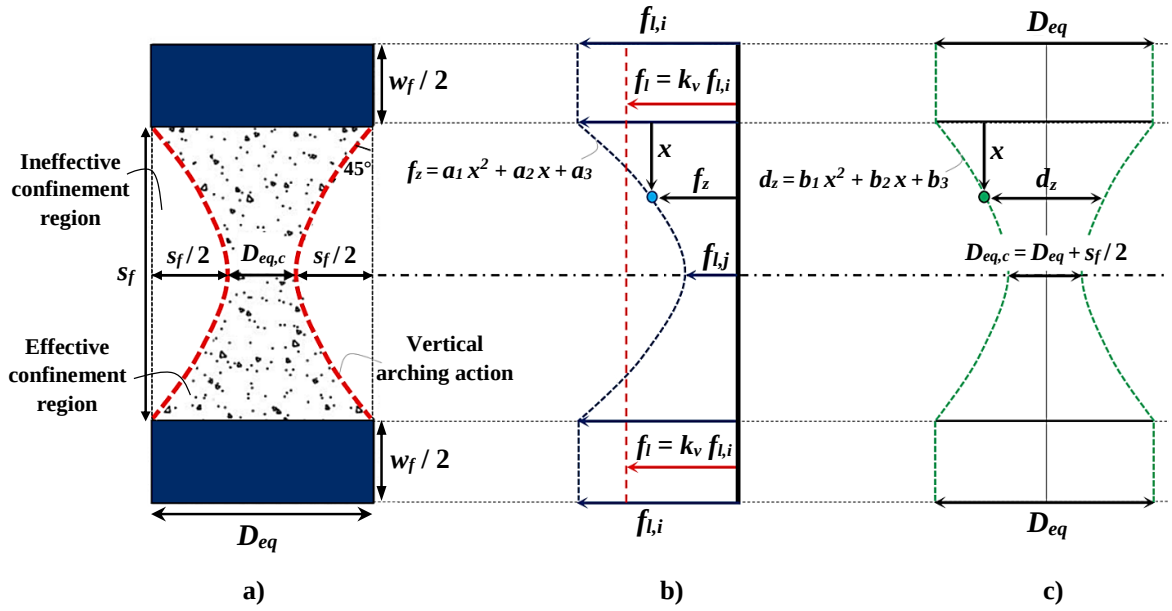

Fig. 3. Vertical arching action phenomenon for partially FRP confined concrete

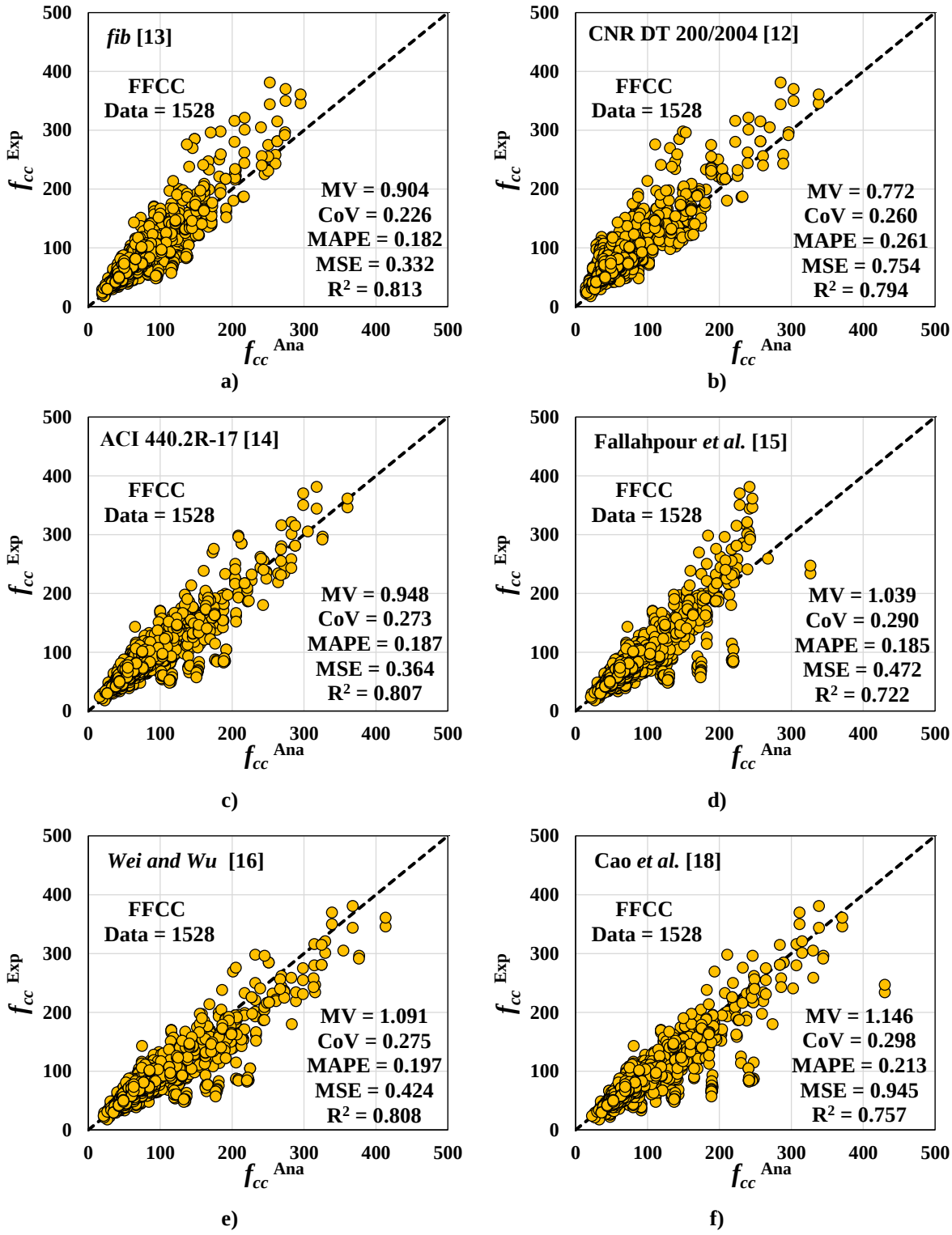
fib [13]
FFCC
Data = 1528
MV = 0.904
CoV = 0.226
MAPE = 0.182
MSE = 0.332
R² = 0.813
a)
CNR DT 200/2004 [12]
FFCC
Data = 1528
MV = 0.772
CoV = 0.260
MAPE = 0.261
MSE = 0.754
R² = 0.794
b)
ACI 440.2R-17 [14]
FFCC
Data = 1528
MV = 0.948
CoV = 0.273
MAPE = 0.187
MSE = 0.364
R² = 0.807
c)
Fallahpour et al. [15]
FFCC
Data = 1528
MV = 1.039
CoV = 0.290
MAPE = 0.185
MSE = 0.472
R² = 0.722
d)
Wei and Wu [16]
FFCC
Data = 1528
MV = 1.091
CoV = 0.275
MAPE = 0.197
MSE = 0.424
R² = 0.808
e)
Cao et al. [18]
FFCC
Data = 1528
MV = 1.146
CoV = 0.298
MAPE = 0.213
MSE = 0.945
R² = 0.757
f)
f_cc Exp
f_cc Ana
0
100
200
300
400
500

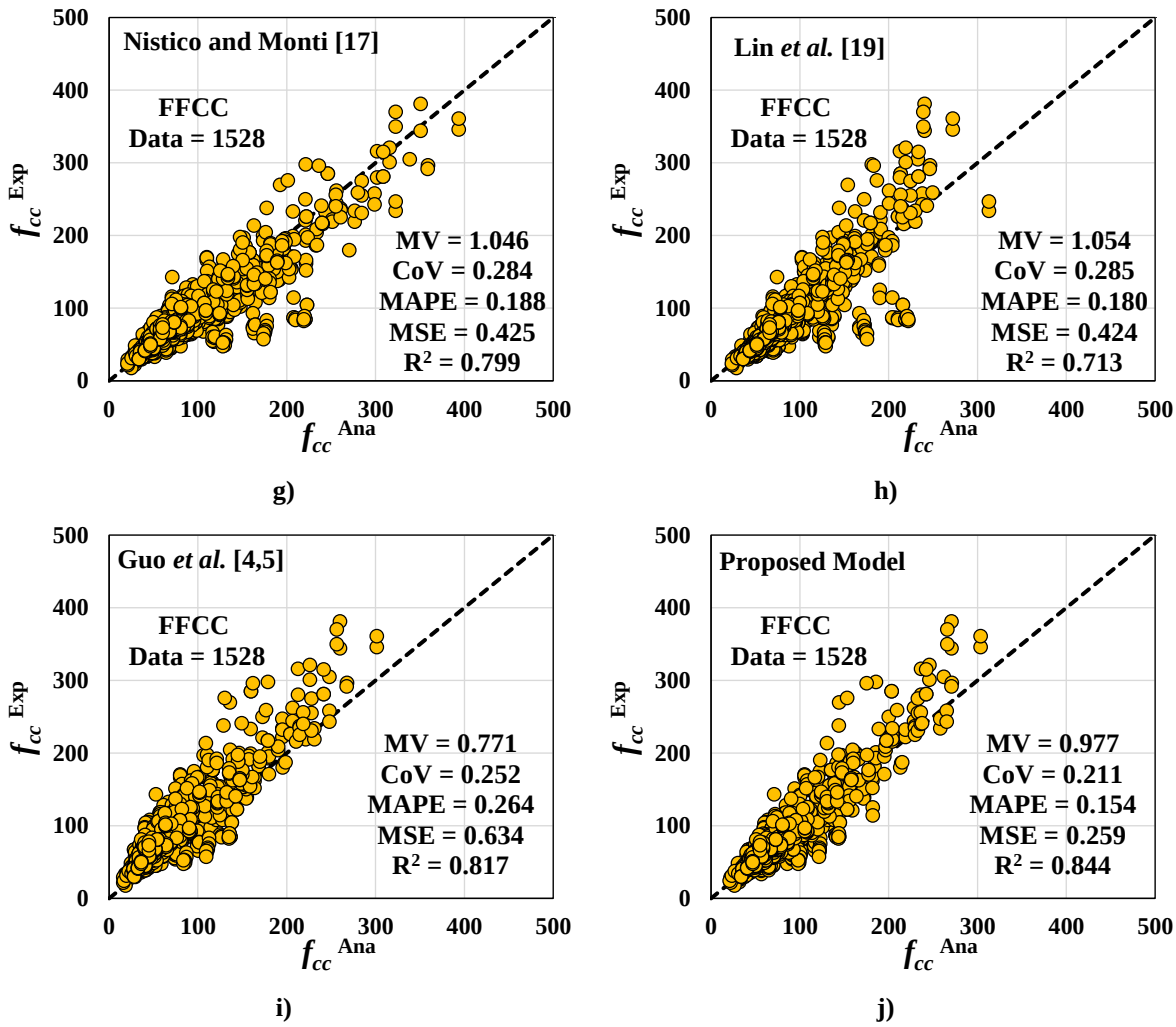

Fig. 4. Axial compressive strength of FFCC: test versus predicted results

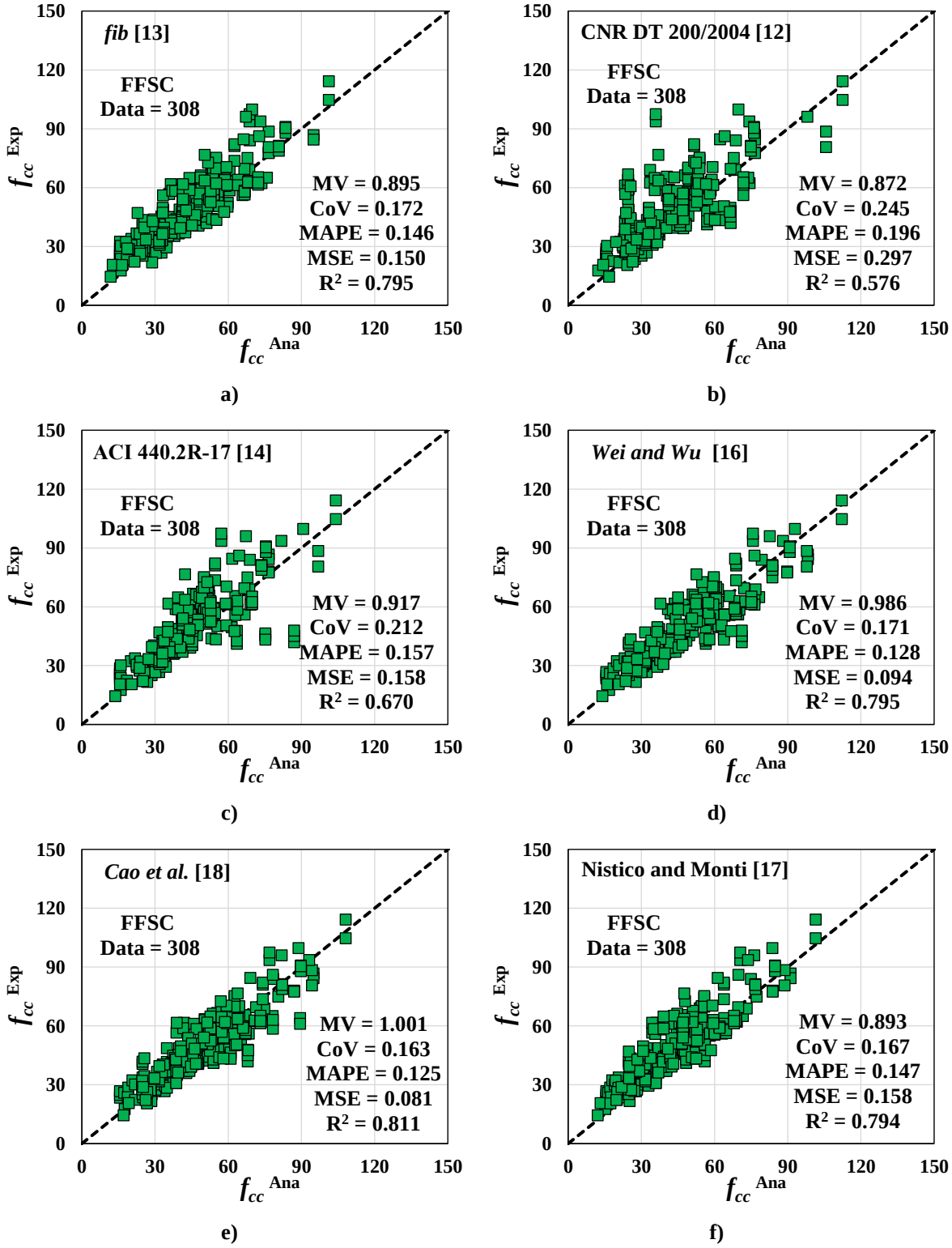
fib [13]
FFSC
Data = 308
MV = 0.895
CoV = 0.172
MAPE = 0.146
MSE = 0.150
R² = 0.795
a)
CNR DT 200/2004 [12]
FFSC
Data = 308
MV = 0.872
CoV = 0.245
MAPE = 0.196
MSE = 0.297
R² = 0.576
b)
ACI 440.2R-17 [14]
FFSC
Data = 308
MV = 0.917
CoV = 0.212
MAPE = 0.157
MSE = 0.158
R² = 0.670
c)
Wei and Wu [16]
FFSC
Data = 308
MV = 0.986
CoV = 0.171
MAPE = 0.128
MSE = 0.094
R² = 0.795
d)
Cao et al. [18]
FFSC
Data = 308
MV = 1.001
CoV = 0.163
MAPE = 0.125
MSE = 0.081
R² = 0.811
e)
Nistico and Monti [17]
FFSC
Data = 308
MV = 0.893
CoV = 0.167
MAPE = 0.147
MSE = 0.158
R² = 0.794
f)
f_cc Exp
f_cc Ana
0
30
60
90
120
150

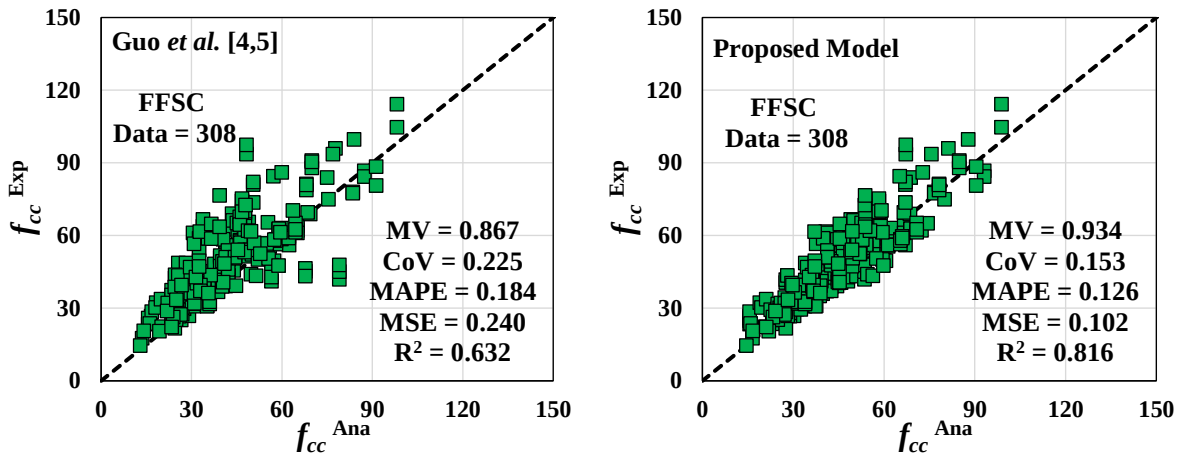

g) h)

Fig. 5. Axial compressive strength of FFSC: test versus predicted results

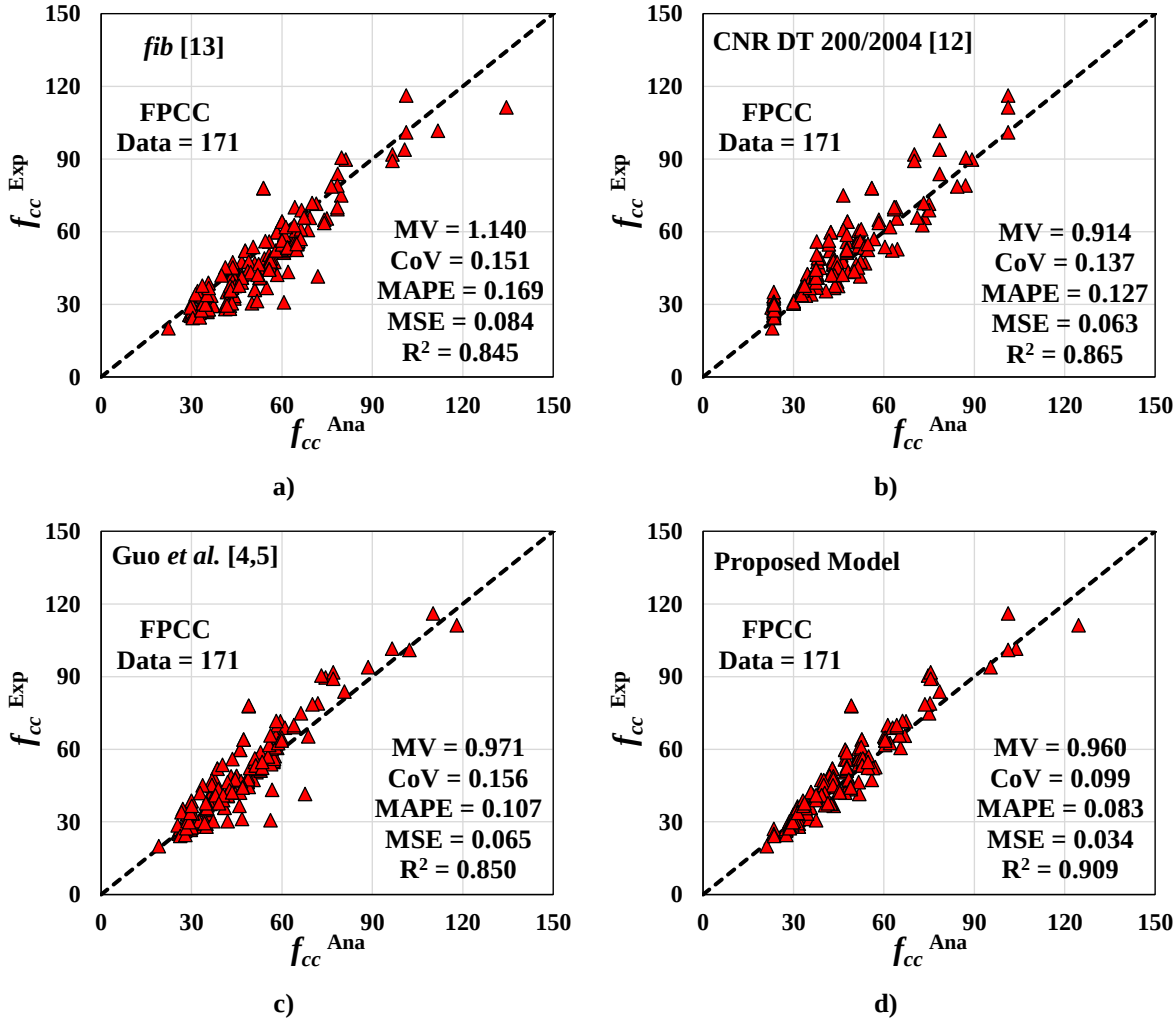

Fig. 6. Axial compressive strength of FPCC: test versus predicted results

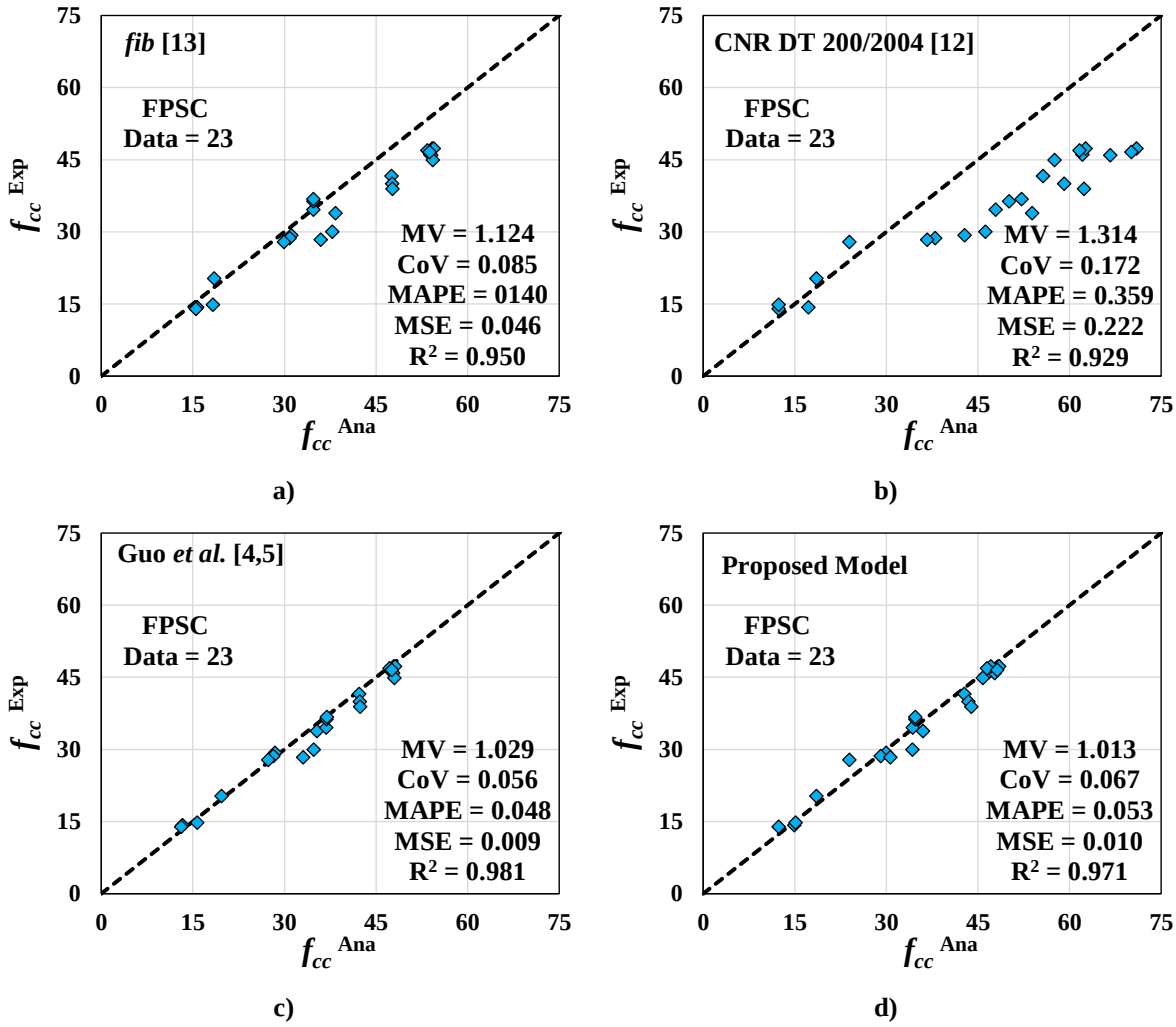

Fig. 7. Axial compressive strength of FPSC: test versus predicted results

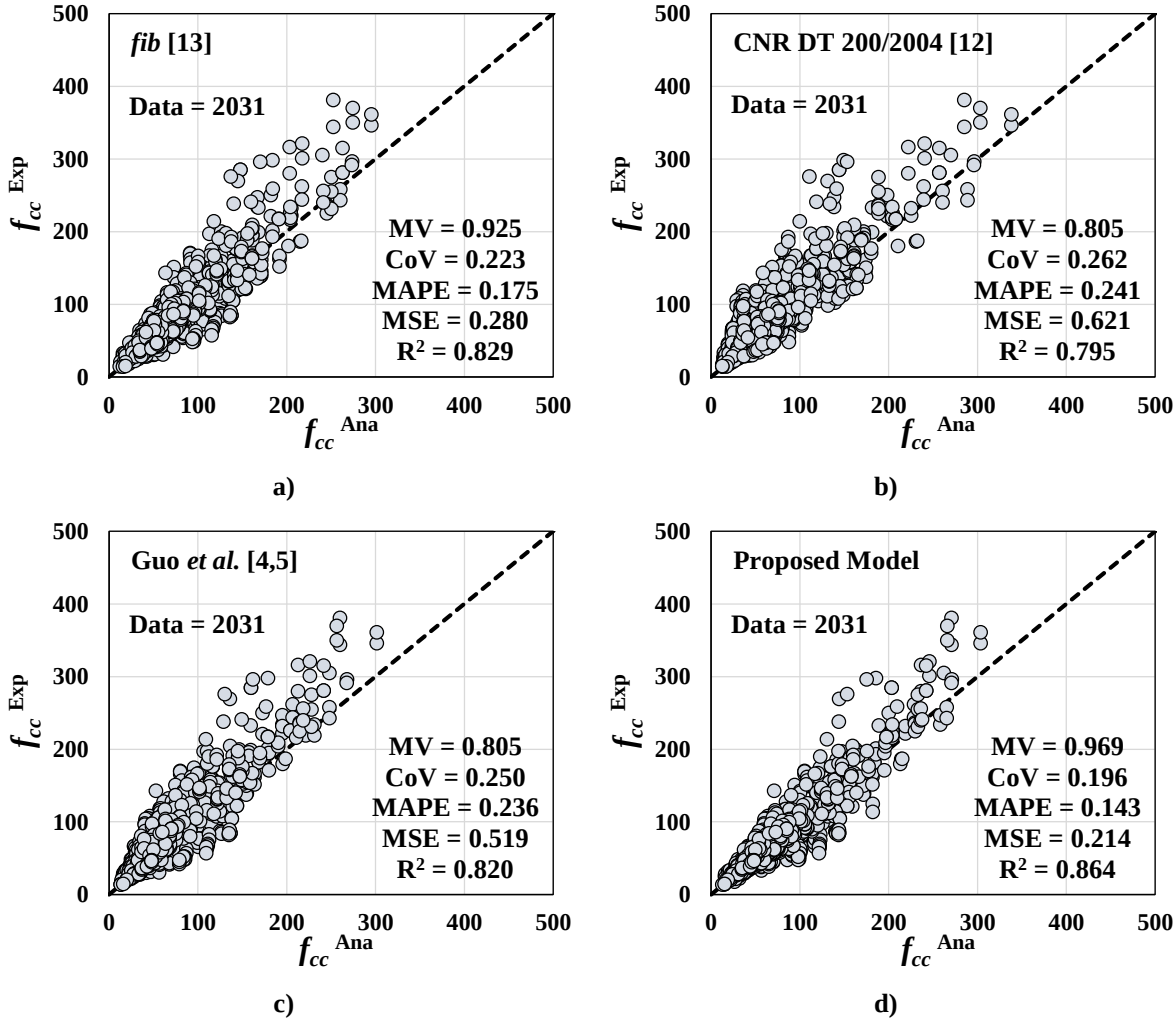

Fig. 8. Axial compressive strength of FFCC/FFSC/FPCC/FPSC: test versus predicted results

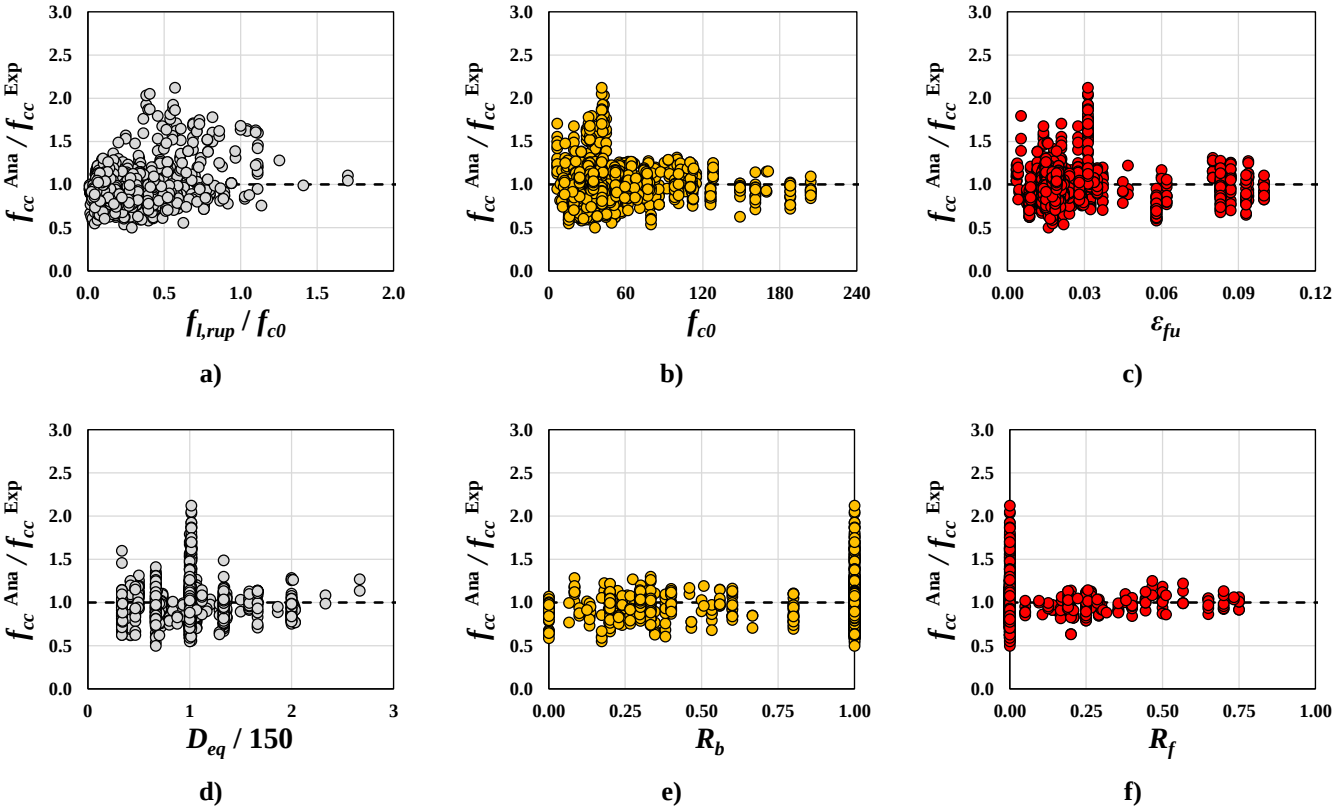

Fig. 9. Performance of the proposed model with respect to key parameters